ISSN 1330-3651 (Print), ISSN 1848-6339 (Online)
https://doi.org/10.17559/TV-20210705101118
Preliminary communication

Strength Degradation Characteristics of the Steel-Concrete Interface Under Cyclic Shear

Mingwei LIU, Fayou WU*, Erdi ABI, Linjian WU, Guangquan SU

Abstract: The shear capacity of the steel-concrete interface (SCI) of concrete-filled steel tubular piles (CFSTs) degrades due to the cyclic shear action of external loading and unloading and can result in a reduction in the bearing capacity. To explore the shear strength degradation characteristics of the steel-concrete interface under cyclic shear, cyclic shear tests for three roughness types and under four different normal stresses were carried out by using a large-scale repeated direct shear test system. The characteristics of the shear load-displacement curve and failure mode of the SCI under external cyclic shear were analyzed, and the influence of the roughness and normal stress on the SCI shear strength degradation was explored. The results indicate that the CFSTs experienced shear failure in the first three shear cycles and then exhibited wear failure. The peak shear load of the SCI increases exponentially with increasing normal stress and decreases logarithmically with increasing cyclic shear time. A larger interfacial roughness and normal stress results in a faster interfacial shear strength ratio (T_{fn}/T_{f1}) weakening during the first three shear cycles, and with an increase of the cyclic shear times, the weakening rate is reduced.

Keywords: degradation characteristics; failure mode; large-scale cycle shear test; roughness; steel-concrete interface

1 INTRODUCTION

In recent years, concrete-filled steel tubular piles (CFSTs) have been widely used in ports, bridges, high-rise buildings and in other engineering fields. CFSTs can give full play to the performance of steel and concrete materials. The concrete core was in a three-way compression state due to the constraint effect of the steel tube, which effectively improves the compressive performance of the concrete and also improves the plasticity and toughness [1-2]. The concrete core can prevent premature local buckling of the steel tubes and ensure the full utilization of the material properties of steel tubes [3-6]. At the same time, compared with ordinary reinforced concrete piles, the size of the CFSTs is significantly reduced [1]. In the construction process, steel pipes can also be used as a template to save considerable time and cost [7-8]. CFSTs are suitable for projects with strict schedule requirements. This advantage has been exploited in the construction of inland river docks in mountainous areas of the upper reaches of the Yangtze River [2]. The cohesion of the steel-concrete interface (SCI) is a key factor that affects the bearing capacity, and plays an important role in load transfer process [9-11]. During the construction of inland river ports in mountainous areas of the upper Reaches of the Yangtze River, such as Guoyuan Port and Luohuang Port in Chongqing, the bonding strength of the interface between steel tube and core concrete was enhanced, and combined work of steel and concrete two-phase materials was realized by welding longitudinal rebars in the inner wall of steel tube (Fig. 1). In the use stage of CFSTs, however, due to the horizontal loads, such as ship berthing impact force and mooring force [12], relative slip may occur between the steel tube and concrete, shear action may exist at the steel-concrete interface with longitudinal rebars, as shown in Fig. 2. The horizontal load acts on the concrete-filled steel tubular pile in a low-frequency and repeated way. Under the cyclic loading, the SCI was subjected to repeated shear action, which resulted in the degradation of the shear strength, and finally the bearing capacity of CFSTs pile was decreased. Therefore, it is necessary to investigate the shear strength degradation characteristics of the SCI under cyclic reversed horizontal loading.

Figure 1 Steel tube of CFST

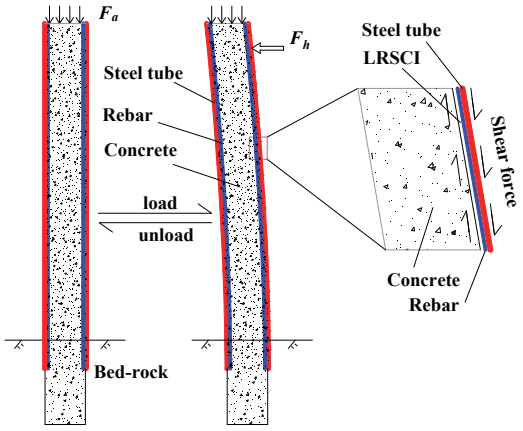

Figure 2 Shear action of CFST

The SCI condition of CFST piles, as an important factor affecting the bearing capacity, has also been widely studied. Hajjar et al. [13], Jin et al. [14], Zhong et al. [15] assumed that both steel tubes and concrete were loaded simultaneously, and the SCI was well bonded such that no sliding occurred. The method proposed by B. Lakshmi et al. [16] to predict the inelastic and ultimate load behavior and the ultimate strength of CFSTs with square, rectangular and circular sections, also assumed that there was an adequate bond between the SCI.

Aval et al. [17] believed that the use of inner ribs or pins could enhance the compounding effect in CFSTs, thus increasing the stress transfer between the steel and concrete.

Xu et al. [11] experimentally concluded that a rougher steel pip inner wall resulted in a better bonding performance. Welded longitudinal ribs on the inner wall of the steel pipe have a significant effect on the interfacial bonding properties of the members. Rodler et al. [18], Maki et al. [19], Heid et al. [20] showed that when the SCI was constrained, the bearing capacity of CFST piles could be improved. Dawn Lehman et al. [8] pointed out that when the SCI shear stress exceeds the bonding stress, relative slip will occur between the core concrete and steel tube, resulting in a decrease in the strength of the CFSTs or the steel tube-reinforced concrete piles. It has also been reported that the bearing capacity of CFSTs can be improved by changing the conditions of the steel-concrete interface. Xu et al. [21] conducted experiments on prestressed concrete-filled circular steel tubes (PCFSTs), compared them with ordinary circular steel tube concrete and pointed out that the core concrete prestress is an important parameter that affects the SCI bond strength. The bond strength of PCFSTs is much greater than that of CFSTs because of the extrusion stress caused by the expansion of expansive concrete. Qu et al. [9] carried out push-out tests on 17 self-compacting concrete-filled steel tube columns considering the interface conditions. Through reasonable design, welded shear studs in steel pipes are believed to improve the interfacial bonding ability and ensure better synergy between the steel pipes and concrete in CFSTs. Zhou et al. [22] explored the bearing capacity of rock-socketed steel H-piles using push-out tests and concluded that under the same conditions, the bearing capacity of H-steel reinforced concrete columns is greatly improved when there are steel tube constraints and bolts at the interface between the H-steel and concrete. These authors also used finite element analysis to define a three-dimensional interface stress element between the steel tube and concrete to simulate the possible slip along the interface. Zhang et al. [2] found that longitudinal reinforcement and concrete filling on the inner side of the steel plate can prevent local instability and improve the bearing capacity of CFSTs. Zhong et al. [3] showed that increasing the number of stiffeners can effectively delay the local buckling of steel pipes and increase the bearing capacity of CFSTs.

To sum up, in the current literature, the adhesion of SCI with the welded circumferential bars or shear stubs was mainly studied by adopting push-out test or push-off test, and the influence of the decrease of adhesion on the bearing capacity of CFST pile was analyzed. The push-out test or push-off test were almost in the way of one-time destruction. The relative slip direction between steel and concrete is mostly perpendicular to the welding direction of reinforcement. However, the mechanical characteristics are different from the SCI of CFST piles used in inland river wharfs in mountainous areas of the upper Reaches of the Yangtze River, and the research on the cyclic shear characteristics of the SCI has not been reported. Therefore, it is necessary to carry out direct shear tests that are parallel to the direction of the welded rebars under low frequency cyclic loading to study the shear degradation characteristics of the SCI.

In this paper, a local small unit on the stress side of CFST piles was selected, the roughness, normal stress and the number of shear cycles were considered, specimens with three different roughnesses and under four different normal stresses were tested by using a large-scale repeated direct shear test system to study the shear performance of SCI. Based on the experiment, the characteristics of shear load-displacement curve and failure mode were analyzed, and the influence of roughness and normal stress on the shear strength degradation of SCI was explored.

2 EXPERIMENTAL STUDY

2.1 Testing Apparatus

The large-scale circulating direct shear test system independently designed and developed by Chongqing Jiaotong University was used for the tests (Fig. 3) The test system consisted of four parts: the base, the sample shear box, the loading system (vertical loading and horizontal cyclic loading), and the test data acquisition and processing system.

The loading system is mainly composed of a computer, hydraulic source, electrohydraulic servo valve and electrohydraulic servo actuator. The sample shear system is composed of an upper shear box, a lower shear box and a roller. The test data acquisition and processing system consist of a measuring sensor, analog controller, computer and other components. Vertical loading, horizontal cyclic loading and data acquisition are all automatically controlled by the computer during the test. The test steps include specimen preparation, specimen installation, vertical loading, horizontal cyclic loading, cyclic shear testing, data acquisition, and data processing.

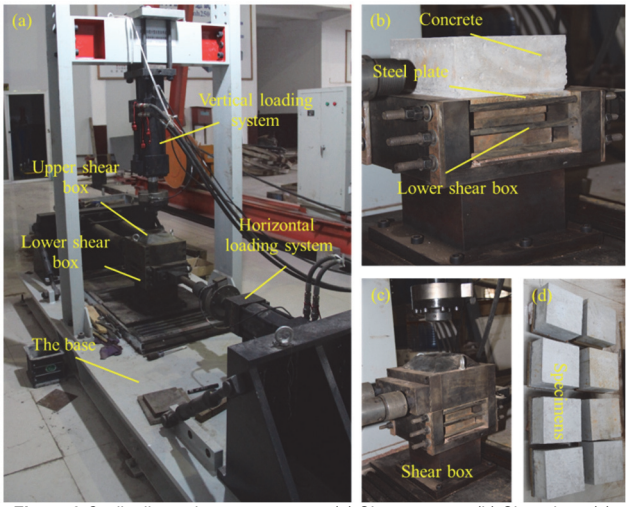

Figure 3 Cyclic direct shear test system: (a) Shear system; (b) Shear box; (c) Shear box; (d) Specimens

2.2 Materials

The test specimen is mainly composed of C30 concrete, steel plate and ribbed bar. According to the "Specification for mix proportion design of ordinary concrete" (JGJ55-2011) [23], C30 concrete has a strength of 38.2 MPa. The specimens were prepared with commercial ordinary Portland flyash cement (P.F 32.5 N). The mix proportions were as follows: Cement: 426 kg/m^3; Fine aggregate (fine sand): 593 kg/m^3; Coarse aggregate (0 - 20 mm stones): 1186 kg/m^3; Water: 195 kg/m^3. Before preparing the test specimens, three standard specimens with dimensions of 150 × 150 × 150 mm were poured with the same mix ratio

as the experimental specimens and then cured for 7 days under the same environmental conditions as the test specimens. Compressive strength test was performed subsequently, and the compressive strength was 26.28 MPa after 7 days of curing, and the mix ratio met the specification requirements.

The steel plate used in the test was a #40 steel plate processed by the Chongqing Banan District Hongli Machinery Parts Factory, located in Chongqing, China. The quality meets the requirements of the national standard "GB/T699-1999 Quality carbon structural steels" [24]. According to technical data provided by the manufacturer, the performances of the steel plate were: Thickness: 20mm, Modulus of Elasticity: 213500 MPa; Yield strength: 341 MPa; Ultimate strength: 580 MPa; Poisson ratio v: 0.28. The surface of the steel plate was ground with a 60-mesh corundum grinding wheel to remove rust before pouring the test specimen.

The ribbed bars were 190mm long and with a diameter of 8 mm. The diameter is large enough to ensure the quality of the welding. Before welding, the ribbed bars were also carefully polished and brightened with a grinder to avoid the influence of corrosion on the bond strength.

2.3 Specimen Preparation

Referring to the direct test of weak structure surface of rock [25], the dimensions of the specimens were designed as 200 × 200 × 100 mm. Three kinds of specimens were designed to simulate different surface roughness of steel concrete, they were no ribbed bar (n = 0), one ribbed bar (n = 1) and two ribbed bars (n = 2), respectively, as shown in Fig. 4.

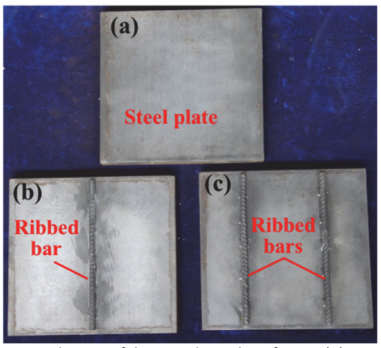

Figure 4 Different roughness of the specimen interfaces: (a) n = 0; (b) n = 1; (c) n = 2

The ribbed bars were welded to the steel plate by arc welding firstly, five welding points were symmetrically and spaced equally arranged on each side of the ribbed bar. After welding, a grinder was used to polish the welded points to avoid stress concentration on the welded joints during the test.

According to the actual engineering ribbed bars layout (Fig. 1), the shear direction is parallel to the welded bars (Fig. 5). To avoid test error caused by contact between the upper shear box and the welded rebar during the test, gap 5 mm wide was set at both ends of the steel bar and along edge of the steel plate. Before pouring the test specimens, plastic strips with a size of 5 × 5 × 200 mm were used to fill the gaps. The specimen model is shown in Fig. 4. The plastic strips were removed after being cured.

2.4 Test Scheme

The specimens were divided into three groups according to the number of ribbed bars at the interface: JQA (n = 0), JQB (n = 1) and JQC (n = 2). There were four specimens in each group, numbered 1, 2, 3 and 4. Constant normal stresses of 200 kPa, 300 kPa, 400 kPa and 500 kPa were adopted during the test. The test scheme is shown in Tab. 1.

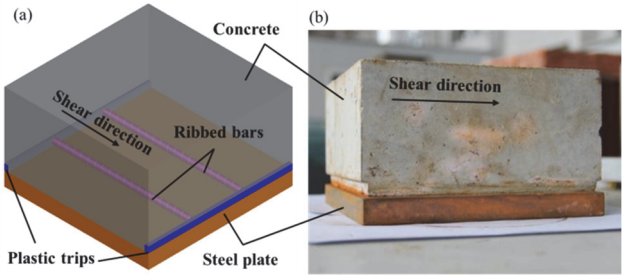

Figure 5 Specimen model diagram: (a) Specimen model; (b) Specimen physical

Table 1 Cyclic shear test scheme

test specimens	rebar number n	normal stress / MPa
JQA-1	0	0.2
JQA-2		0.3
JQA-3		0.4
JQA-4		0.5
JQB-1	1	0.2
JQB-2		0.3
JQB-3		0.4
JQB-4		0.5
JQC-1	2	0.2
JQC-2		0.3
JQC-3		0.4
JQC-4		0.5

There have been a few reports on direct shear tests of SCI. Referring to ASTM D5321, a displacement-controlled loading scheme was adopted for all tests. The cyclic direct shear test (CDS) was sinusoidal displacement-controlled tested with a semi-amplitude of ±2.5 mm. The sample was translated horizontally following the shear paths shown in Fig. 6 and consisted of four processes: (I) - (II) - (III) - (IV).

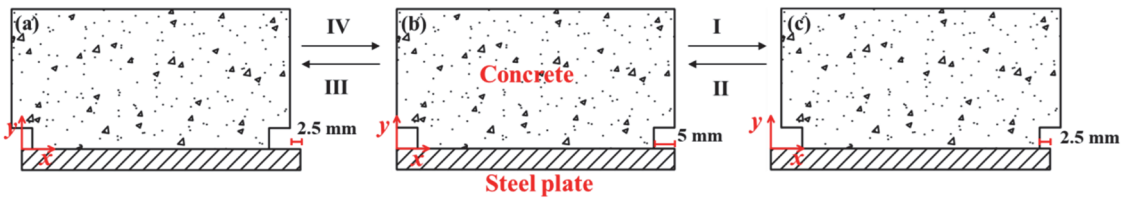

Figure 6 Cyclic shear path: (a) Shear displacement = -2.5 mm; (b) Initial position = 0 mm; (c) Shear displacement = +2.5 mm

3 ANALYSIS OF TEST RESULTS

3.1 Curve Characteristics of the Shear Load-Displacement of a Single Shear Cycle

Fig. 7 shows the shear load (*SL*) versus shear displacement (*SD*) loop curves of the first shear cycle for each specimen. Herein, the mean values of the semi-amplitude shear load of every cycle correspond to the cyclic shear load of the SCI.

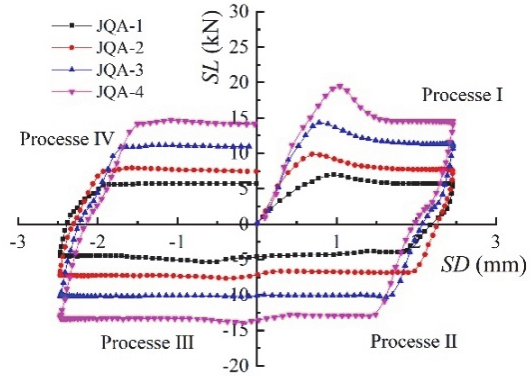

(a) Specimen JQA

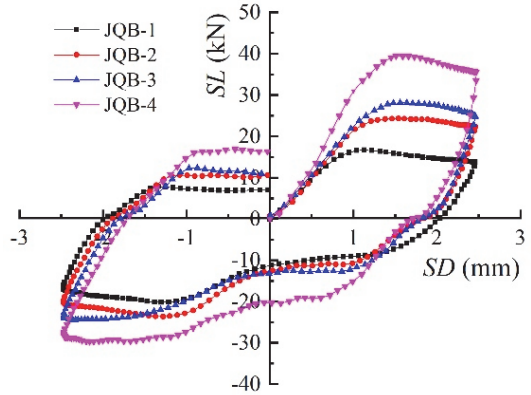

(b) Specimen JQB

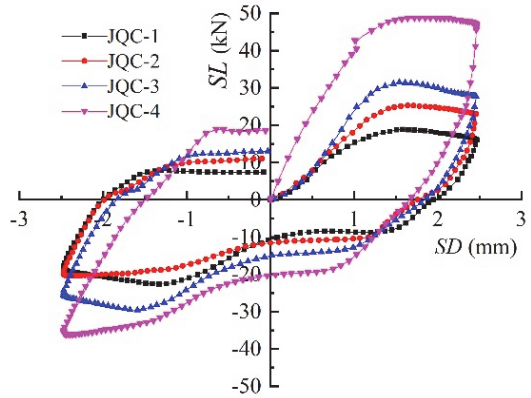

(c) Specimen JQC

Figure 7 Shear load-displacement of a single shear cycle

Fig. 7a shows the first cyclic shear load-displacement curves for the four specimens in the JQA group under different normal stresses. The curves of the four specimens under different normal stresses followed the same trend. In process I, the shear load gradually increased to reach the peak value, and then, the shear load drops to a constant value and remains unchanged until the end of the controlled shear displacement. In the subsequent three processes, the shear load did not appear to have a peak value and remained unchanged after reaching a certain value.

Fig. 7b and Fig. 7c are the shear load-displacement diagrams of JQB and JQC under different normal stresses during the first shear cycle, respectively. The shear load displacement curve trends for both sets of specimens under four normal stresses are similar. A peak value occurred in process I and process III, and after reaching a peak, there was a slight decrease until the controlled shear displacement. The difference between the two sets of tests is that the peak values under the same normal stress are different. The shear loads of the specimens tested under the same normal stress in JQC are greater than those of JQB.

The peak shear load of the first shear cycle of each specimen under different normal stresses is shown in Fig. 8. The peak shear load increased with increasing normal stress. For the JQA, JQB and JQC specimens, the normal stress increased from 200 kPa to 500 kPa, and the peak shear load increased by 176.81%, 136.83% and 159.03%, respectively. Fig. 9 shows the curve of the shear strength growth rate with an increase in the number of interfacial reinforcing bars. Under the same normal stress, when the number of reinforcing bars increased from 0 to 1, the interfacial shear strength increased significantly. When the number of bars increased from 1 to 2, the interfacial shear strength rate of increase slowed down.

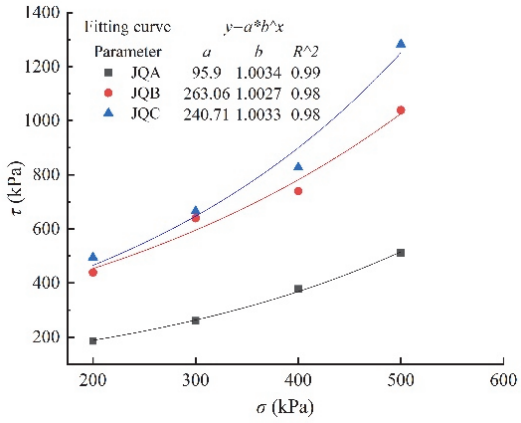

Figure 8 Initial shear stress - normal stress curves for specimens JQA, JQB and JQC

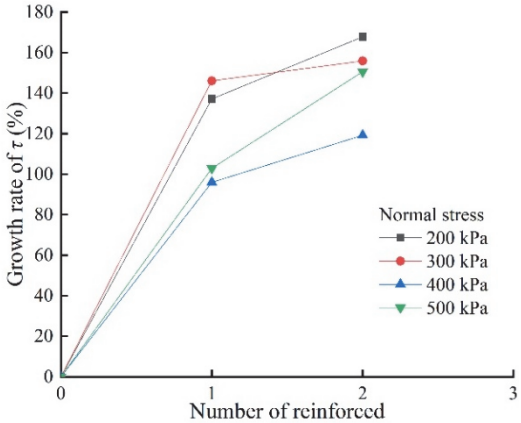

Figure 9 Shear stress rate - number of reinforcement curves

The shear stress is a single-valued function of the normal stress, and the shear stress can be calculated by Eq (1):

$$\tau=\frac{F_{f1}}{A}=f(\sigma) \tag{1}$$

where F_{f1} is the first shear peak load (kN), and A represents the shear area (m^2).

From Fig. 8, it is evident that the peak shear load varied nonlinearly with the normal stress. To quantify the extent of nonlinearity in the normal stress behavior, a logarithmic relationship is applied here and expressed as Eq. (2):

$$\tau=a\times b^{\sigma} \tag{2}$$

where a and b are the fitting coefficients.

Fig. 9 shows that more welded rebar welded and a greater normal stress resulted in a higher peak shear load. Moreover, the shear resistance significantly increased when there is one rebar. The rebar increased from 1 to 2, the increase in additional shear strength is relatively insignificant.

3.2 Characteristics of the Shear Load-Displacement Curve Under Multiple Shear Cycles

In the cyclic direct shear test, the shear load-shear displacement curves after 10 shear cycles almost overlap, therefore, the first 10 shear cycles are taken for analysis. Fig. 10 shows the shear load-shear displacement curves of the first 10 cycles under different normal stresses for the three samples.

During the first 1 to 3 shearing cycles for sample JQA, the shear load of the sample first increased and then decreased with increasing shear displacement (Fig. 10a). The shear load-displacement curve exhibited obvious peak values in processes I and III. The peak shear load gradually decreased with increasing shear cycles. The peak load characteristics of the curve began to disappear and gradually tended to the residual load as the number of cycles increased. In the subsequent 4 - 10 shear cycles, the SCI shear load-displacement curve basically overlaps into a single curve. The peak load of the sample is almost equal to the residual load.

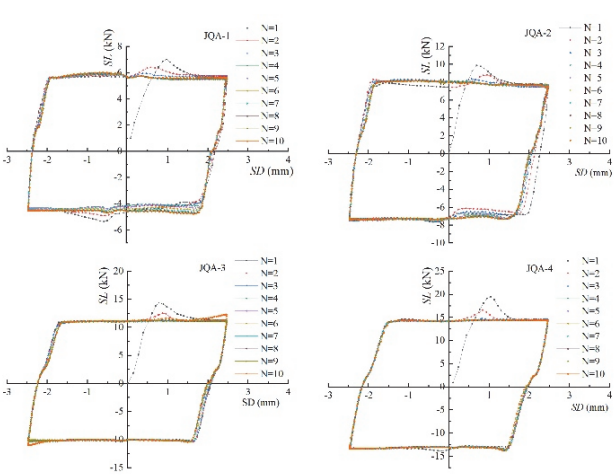

(a) Shear load-displacement curve for specimen JQA

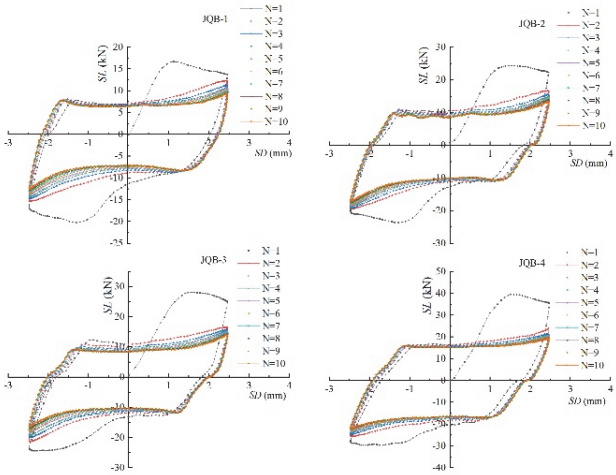

(b) Shear load-displacement curve for specimen JQB

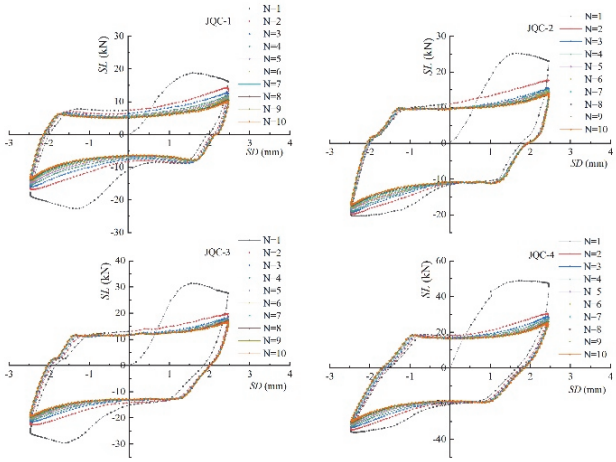

(c) Shear load-displacement curve for specimen JQC

Figure 10 Shear load-displacement curve for 10 cyclic shear cycles

The characteristics of the cyclic shear load-displacement curves of samples JQB and JQC are similar. The maximum shear load was observed in the first cycle and decreased nonlinearly with increasing cycle number, which indicates that the SCI was characterized by softening with increasing cycle number (Fig. 10b and Fig. 10c).

4 DISCUSSION

4.1 Failure Mode Analysis

Xue and Cai [26] proposed a simplified two-stage elastoplastic bond strength slip model using reverse push-out tests, and Liu [10] proposed a three-stage bond strength

slip model based on a square CFSTs also based on a push-out test. Additionally, through push-out experiments, the 4 stage bond strength slip model was proposed by Qu and Liu [9], Qu [27]. Based on previous research and the shear load displacement curves obtained from this test (Fig. 7 and Fig. 10), the SCI failure modes can be divided into two types: shear failure and wear failure, as shown in Fig. 11. The *SL-SD* curve can be divided into three stages when the specimen is in the shear failure state: there are obvious increasing zone, peak zone and slip zone. There is a large difference between the peak shear load and the residual shear load. The *SL-SD* curve mainly presents two stages when the sample is undergoing wear failure: increasing zone and slip zone. The difference between the peak strength and the residual strength is not obvious.

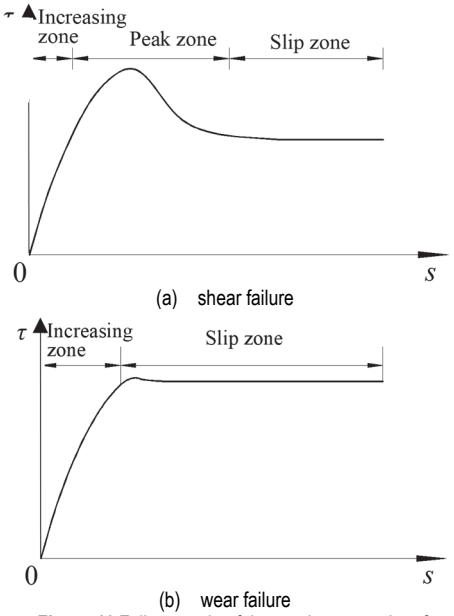

Figure 11 Failure mode of the steel concrete interface

This is because the interface force of the steel concrete is mainly composed of a chemical bonding force, mechanical biting force and friction force [28-29]. In the initial stage of the test, these three forces resist the shear load together. The chemical bonding force is gradually lost in the first few cyclic shear of the test due to the relatively weak shear resistance, and then the SCI shear resistance is composed of a friction force and a residual mechanical biting force.

In the first shear cycle curve of JQA (Fig. 7a), the increasing zone, peak zone and slip zone of the specimen in process I are obvious, indicating shear failure. In the II-IV shear process, the peak area is not obvious, showing wear failure. The single cyclic shear load displacement curve for JQB is similar to that of JQC, as shown in Fig. 7b and Fig. 7c. In process I and process III, the shear mode is shear failure, and the test curve has the characteristic of peak strength, but there is no obvious residual strength, only showing the increasing zone and part of the peak zone. The reason for this is that a displacement control method was adopted in the test, and the maximum shear displacement during the shear process was 2.5 mm, which was not enough for the shear load-shear displacement curve to reach the slip zone. In process II and process IV, the shear load-shear displacement curve remains flat, and there is no peak value, showing the wear stage. The reason for this is that process II and process IV are the processes of the specimen being restored to its original state.

The interface of the JQA sample is composed of steel and concrete, the chemical bond strength and mechanical bite force quickly decrease after the first three cycles, and the shear resistance is transformed into a stable frictional resistance. Therefore, the shear load displacement curve immediately enters the slip zone after the increasing zone, and the failure mode transitions from shear failure to wear failure, as shown in Fig. 10a. The roughness of the SCI in samples JQB and JQC increased due to the rebar welding, and the effect of the mechanical biting force is enhanced, as shown in Fig. 12. In the first three shear cycles, the chemical bond force gradually disappeared, and the concrete trapped in the micro-concave and convex parts of the steel plate and between the steel bar ribs began to shear and crush. The reinforced rib with high stiffness repeatedly extrudes and abrades the concrete, which causes the concrete to fracture and break. The shear load displacement curve presents shear failure mode. With the increase in the cyclic shear time, the micro-convex peaks of concrete continue to fracture, and the mechanical biting force gradually loses. The shear strength of the interface is borne by the friction force, and the failure mode transitions from shear failure to wear failure.

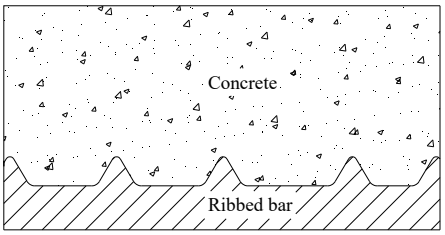

Figure 12 Contact surface of the reinforced concrete

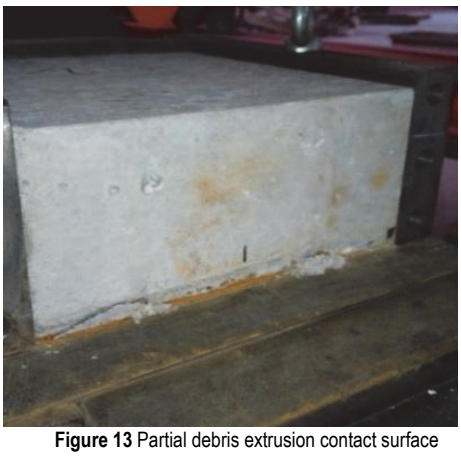

Figure 13 Partial debris extrusion contact surface

After several repeated cyclic shear cycles, the concrete was ground into debris and to powder, and part of the debris extruded out of the interface (Fig. 13). And part of the debris extruded and slipped into the shear interface during the shear process, which increases the friction force at the interface and leads to an increase in the shear load. This explains why the test curves in Fig. 10b and Fig. 10c are not close to a straight line in process I and process III after shear failure, but increase with increasing shear displacement.

In general, in the first three shear cycles, the interface

failure form is shear failure. With the increase in the number of shear cycles, the failure mode turns to wear failure.

4.2 Influencing Factors for the Shear Strength Degradation of the Steel Concrete Interface

4.2.1 Number of Cyclic Shear

Fig. 14 shows the peak shear load-cycle number curve for each of the first 10 cycles for the three specimen groups. In the first 1-3 cycles for each specimen, the peak shear load decreases sharply. More rebar and a higher normal stress result in a greater reduction in the peak load. After the third cycle, the peak shear load tends to be flat, and the reduction range is very small.

In conclusion, under the condition of a displacement-controlled shear test, the degradation of the peak shear strength of SCI mainly occurs during the first three cycles, and the degradation between the first cycle and the third cycle is particularly significant. The reason for this is that the chemical bonding between the SCI and the larger convex peak is destroyed at this stage, such that the chemical bonding force and part of the mechanical biting force are quickly lost. Comparing the curves from JQA, JQB and JQC, the shear strength of JQA is mainly borne by the friction force and chemical bonding force between interfaces because there is no ribbed bar. The shear strength of the mechanical biting force is relatively weaker, so the peak strength of the JQA group is far less than that of JQB and JQC.

A logarithmic function was used to describe the degradation behavior of the peak shear load of each specimen as a function of the number of shear cycles, as shown in Fig. 14. They all fit well, and the equation is as follows:

$$F_{fn} = a - b \times \ln(N + c) \tag{3}$$

where a, b and c are the fitting coefficients, and N is the number of shear cycles.

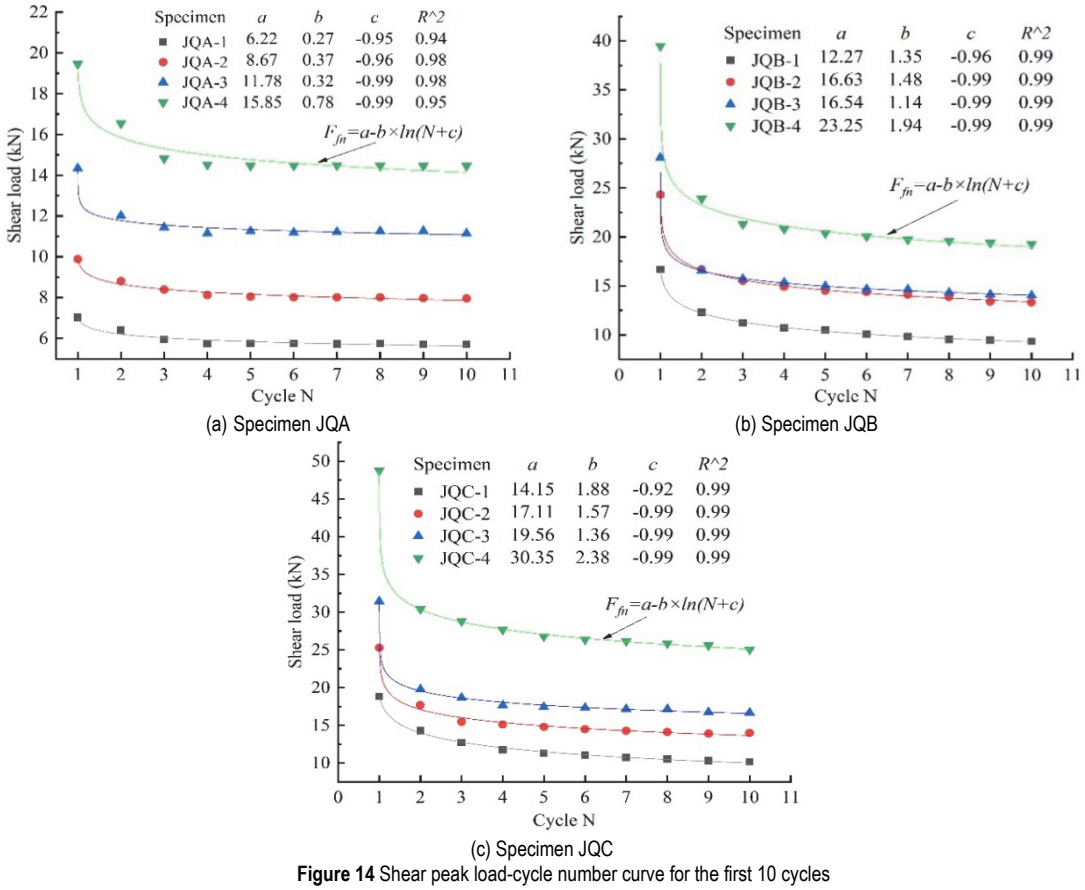

(a) Specimen JQA

(b) Specimen JQB

(c) Specimen JQC

Figure 14 Shear peak load-cycle number curve for the first 10 cycles

4.2.2 Interface Roughness

To intuitively reflect the shear strength degradation characteristics for different interface roughness as a function of the number of shear cycles, the shear strength ratio R_τ of the SCI under cyclic shear loading is defined as Eq. (4):

$$R_\tau = \frac{\tau_{fn}}{\tau_{f1}} \tag{4}$$

where τ_{fn} is the peak shear strength of the Nth shear cycle, and τ_{f1} refers to the peak shear strength of the first shear cycle.

The peak shear strength is the ratio of the peak shear load to the shear area, so Eq. (4) can be converted into Eq. (5):

$$R_\tau = \frac{\tau_{fn}}{\tau_{f1}} = \frac{\left(F_{fn} / A\right)}{\left(F_{f1} / A\right)} = \frac{F_{fn}}{F_{f1}} \tag{5}$$

where F_{fn} indicates the peak shear load of the Nth shear cycle, and F_{f1} represents the peak shear strength of the first shear cycle.

The definition shows that as R_τ approaches 1, less shear strength degradation occurred on the SCI. A smaller R_τ value indicates a serious degree of shear strength degradation.

The variation of the SCI shear strength ratio with the number of shear cycles is shown in Fig. 15. Under the same normal stress, the R_τ of the three interfacial roughness samples decreases with an increase in the number of shear cycles. The R_τ of specimen JQA decreases slowest with an increase in the number of cycles. After three shear cycles, R_τ remains constant, that is, the peak shear load at the interface tends to be constant. The R_τ values for samples JQB and JQC decrease with an increase of shear cycle times, and continue to decrease slightly over all 10 shear cycles. The rate decrease of R_τ for samples JQB and JQC is obviously faster than that of JQA. The R_τ of sample JQA decreased by an average of 7.0% in each of the first three shear cycles and 0.12% in the fourth to tenth shear cycles. The R_τ of samples JQB and JQC decreased by 13.93% and 13.74%, respectively, in each of the first three shear cycles and 0.10% and 0.9%, respectively, in the fourth to tenth shear cycles. The results show that the degradation of R_τ occurs mainly during the first three cyclic shear cycles. A greater SCI surface roughness results in a greater degradation degree during the first three cyclic shear cycles and in the subsequent shear; however, R_τ decreases slightly.

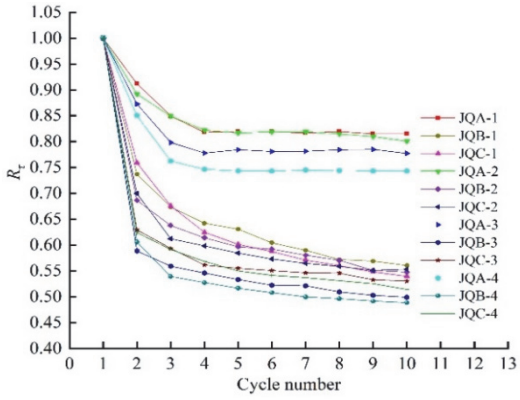

Figure 15 Variation in R_τ with the number of cycles

According to the analysis, a greater SCI roughness results in a faster R_τ decay in each of the first three cyclic shear cycles. However, the results also show that a greater steel-concrete interface roughness results in a greater shear load.

4.2.3 Normal Stress

Fig. 15 also shows the degradation rule of R_τ with the cyclic shear times under the same roughness but for different normal stresses. The variation trend of R_τ of the samples with the same interface roughness under different normal stresses is also similar: R_τ decays rapidly in the first 3 cyclic shear cycles and subsequently decreases slowly. Under the same interface roughness, the average degradation of R_τ in the first three cycles is 10.18%, 10.74%, 12.39% and 13.24% when the normal stress ranges from 0.2 MPa to 0.4 MPa, and the average degradation of R_τ in the subsequent cycles is 0.94%, 0.74%, 0.44% and 0.53%, respectively. Under different normal stresses, degradation mainly occurred during the first three cyclic shear cycles, and a greater normal stress resulted in a greater degradation degree. However, a greater normal stress resulted in a greater shear load. This indicates that a greater roughness and normal stress result in better shear performance of the steel concrete interface.

5 CONCLUSIONS

In the current work, the SCI was studied by considering the influence of the roughness, normal stress and number of cycles, and large-scale direct shear tests were carried out to explore the shear strength degradation characteristics. The characteristics of the *SL-SD* curves and SCI failure mode under external cyclic shear were analyzed, and the influence of roughness and normal stress to the degradation of shear strength was also explored. The conclusions are summarized below:

(1) Under the displacement-controlled shear test, the peak shear load of the steel concrete interface increases exponentially with increasing normal stress given the same interface roughness.

(2) The shear load of SCI degraded faster with increasing cyclic shear number, roughness and normal stress. The peak shear load increased exponentially with increasing normal stress and decreased logarithmically with increasing cycle number.

(3) The failure modes of the steel concrete interface are divided into shear failure and wear failure, and the shear failure is divided into an increasing zone, a peak zone and a slip zone. The wear failure is divided into an increasing zone and a sliding zone. During the initial 3 shear cycles, the SCI failure mode was shear failure, and the specimen subsequently transformed into wear failure.

(4) Welding longitudinal rebars on the inner wall of the steel tube can also attribute to improve the bonding state between the steel tube and core concrete, but not all designing welded rebars contributed to the increment of bond strength. Study about the influence of the number, diameter and arrangement of rebar on the bond mechanism need to be further researched.

Acknowledgments

The research reported in this paper has been supported by the National Natural Science Foundation of China (No.51479014) and the National Key Research and Development Program of China (2018YFB1600400), and Sichuan Provincial Communications Department Project (No.2018-B-04). The Talents Plan Project in Chongqing of China (cstc2021ycjh-bgzxm0053). The Research Innovation Project for Graduate Students in Chongqing of China (CYS20300). The financial support is highly appreciated.

6 REFERENCES

[1] Lam, D. & Gardner, L. (2008). Structural design of stainless steel concrete filled columns. *Journal of Constructional Steel Research*, *64*(11), 1275-1282. https://doi.org/10.1016/j.jcsr.2008.04.012

[2] Zhang, X., Duan, B., Wang, C., & Wang, D. (2019). Dynamic response analysis of lateral impact force of frame wharf with rock-socketed piles in inland river steel sheath. *Advances in Civil Engineering*, *2019*(1), 1-15. https://doi.org/10.1155/2019/6918376

[3] Zhong, T., Han, L. H., & Wang, D. Y. (2008). Strength and ductility of stiffened thin-walled hollow steel structural stub columns filled with concrete. *Thin Walled Structures*, *46*(10), p.1113-1128. https://doi.org/10.1016/j.tws.2008.01.007

[4] Zhang, J. G., Liu, Y. J., Yang, J., & Xu, K. L. (2011). Experimental research and finite element analysis of concrete-filled steel box columns with longitudinal stiffeners. *Advanced Materials Research*, 287-290, 1037-1042. https://doi.org/10.4028/www.scientific.net/AMR.287-290.1037

[5] Zhou, Z., Gan, D., & Zhou, X. H. (2019). Improved composite effect of square concrete-filled steel tubes with diagonal binding ribs. *Journal of Structural Engineering*, *145*(10). https://doi.org/10.1061/(ASCE)ST.1943-541X.0002400

[6] Dabaon, M., El-Khoriby, S., El-Boghdadi, M., & Hassanein, M. F. (2009). Confinement effect of stiffened and unstiffened concrete-filled stainless steel tubular stub columns. *Journal of Constructional Steel Research*, *65*(8), 1846-1854. https://doi.org/10.1016/j.jcsr.2009.04.012

[7] Zhang, Y. T., Shan, B., & Xiao, Y. (2019). Axial impact behaviors of stub concrete-filled square steel tubes. *Advances in Structural Engineering*, *22*(3), 136943321984509. https://doi.org/10.1177/1369433219845094

[8] Lehman, D., Roeder, C., Heid, A., Maki, T., & Khaleghi, B. (2018). Shear response of concrete filled tubes part 1: experiments. *Journal of Constructional Steel Research*, *150*(NOV.), 528-540. https://doi.org/10.1016/j.jcsr.2018.08.027

[9] Qu, X. S. & Liu, Q. (2017). Bond strength between steel and self-compacting lower expansion concrete in composite columns. *Journal of Constructional Steel Research*, *139*, 176-187.https://doi.org/10.1016/j.jcsr.2017.09.017

[10] Liu, Y. Q. (2006). *Study on the Basic Theory of Bond-Slip between Steel Tube and Concrete in CFT Structures and Numerical Simulation by ANSYS Program*. M.A. Thesis. Xi'an: Xi'an University of Architecture and Technology. (In Chinese)

[11] Xu, K. C., Huang, C., & Chen, M. (2013). Research on impact of steel tube inner surface roughness on interfacial bonding behavior of cfst. *JianzhuJiegouXuebao/Journal of Building Structures*, *34*(S1), 420-424.

[12] Li, Y., Lence, B. J., Zhou, S. L., & Wu, Q. (2011). Stochastic Fatigue Assessment for Berthing Monopiles in Inland Waterways, *Journal of Waterway Port Coastal & Ocean Engineering*, *137*(2), 43-53. https://doi.org/10.1061/(ASCE)WW.1943-5460.0000063

[13] Hajjar, J. F. & Gourley, B. C. (1996). Representation of concrete-filled steel tube cross-section strength. *Journal of Structural Engineering*, *122*(11), 1327-1336. https://doi.org/10.1061/(ASCE)0733-9445(1996)122:11(1327)

[14] Jin, L., Fan, L., Li, P., & Du, X. Size effect of axial-loaded concrete-filled steel tubular columns with different confinement coefficients. *Engineering Structures*, *198*, 109503-109503. https://doi.org/10.1016/j.engstruct.2019.109503

[15] Zhong, T., Wang, Z. B., & Yu, Q. (2013). Finite element modelling of concrete-filled steel stub columns under axial compression. *Journal of Constructional Steel Research*, *89*(oct.), 121-131. https://doi.org/10.1016/j.jcsr.2013.07.001

[16] Lakshmi, B. & Shanmugam, N. E. (2002). Nonlinear analysis of in-filled steel-concrete composite columns. *Journal of Structural Engineering, 128* (7): 922-933. https://doi.org/10.1061/(ASCE)0733-9445(2002)128:7(922)

[17] Aval, S., Saadeghvaziri, M. A., &Golafshani, A. A. (2002). Comprehensive composite inelastic fiber element for cyclic analysis of concrete-filled steel tube columns. *Journal of Engineering Mechanics*, *128*(4), 428-437. https://doi.org/10.1061/(ASCE)0733-9399(2002)128:4(428)

[18] Roeder, C. W., Lehman, D. E., & Bishop, E. (2010). Strength and stiffness of circular concrete-filled tubes. *Journal of Structural Engineering*, *136*(12), 1545-1553. https://doi.org/10.1061/(ASCE)ST.1943-541X.0000263

[19] Maki, T. R. (2015). *Experimental Investigation of the Shear Resistance of Circular Concrete-Filled Steel Tubes (CFTs) Subjected to Transverse Loading*. M.A. Thesis. Seattle: University of Washington.

[20] Heid, A. E. (2016). *Shear Resistance of Circular Concrete-Filled Steel Tubes*. M.A. Thesis. Seattle: University of Washington.

[21] Chang, X., Huang, C. K., Jiang, D. C., & Song, Y. (2009). Push-out test of pre-stressing concrete filled circular steel tube columns by means of expansive cement. *Construction & Building Materials*, *23*(1), 491-497. https://doi.org/10.1016/j.conbuildmat.2007.10.021

[22] Zhou, Y. D., Tham, L. G., Tang, X. W., Liu, Y. T., & Wong, M. K. (2011). Parametric analyses of push-out tests and implications for design of rock-socketed steel h-pile. *Computers & Geotechnics*, *38*(3), 383-392. https://doi.org/10.1016/j.compgeo.2011.01.002

[23] China Academy of Building Research. (2011). *Specification for mix proportion design of ordinary concrete (JGJ55-2011)*. Beijing:China Architecture & Building press.

[24] The state bureau of quality and technical supervision. (1999). Quality carbon structural steels (GB/T699-1999). Beijing: Standards Press of China.

[25] MOHURD, The state bureau of quality and technical supervision. (2013). Standard for test methods of engineering rock mass (GB/T50266-2013). Beijing, China Planning Press.

[26] Xue, L. (1998). Experimental study on shear connectors of concretefilled steel tube. *BUILDING SCIENCE*., *14*(1), 13-21.

[27] Qu, X. S. (2011). *Research on Cooperativity and Composite Mechanical Performance for Rectangular Concrete-filled Steel Tubular Columns.* Ph.D. Dissertation. Tianjin: Tianjin University.

[28] Lutz, L. & Gergely, P. (1967). Mechanics of bond and slip of deformed bars in concrete. *Aci Journal*, *64*(11), 711-721. https://doi.org/10.14359/7600

[29] Stocker, M. F. & Sozen, M. A. (1970). Investigation of Pre-stressed Reinforced Concrete for Highway Bridges. Part V: Bond Characteristics of Pre-stressing Strand. *University of Illinois Bulletin* No.503, University of Illinois at Urbana-Champaign, Urbana, IL, 116-119.

Contact information:

Mingwei LIU, PhD, Professor
National Engineering Research Center for Inland Waterway Regulation, School of River and Ocean Engineering,
Chongqing Jiaotong University,
66 Xuefu Road, Nan'an District,
Chongqing 400074, P. R. China
Mobile phone: +86 13452012420
E-mail: mingwei_liu@126.com

Fayou WU, PhD candidate
(Corresponding author)
National Engineering Research Center for Inland Waterway Regulation, School of River and Ocean Engineering,
Chongqing Jiaotong University,
66 Xuefu Road, Nan'an District,
Chongqing 400074, P. R. China
People's Republic of China
Mobile phone: +86 18723376585
E-mail: wfyou2020@126.com

Erdi ABI, PhD, Associate Professor
National Engineering Research Center for Inland Waterway Regulation, School of River and Ocean Engineering,
Chongqing Jiaotong University,
66 Xuefu Road, Nan'an District,
Chongqing 400074, P. R. China
People's Republic of China
Mobile phone: +86 15696202667
Email: abierdi@163.com

Linjian WU, PhD, Post-Doctor, Associate Professor
National Engineering Research Center for Inland Waterway Regulation, School of River and Ocean Engineering,
Chongqing Jiaotong University,
66 Xuefu Road, Nan'an District,
Chongqing 400074, P. R. China
People's Republic of China
Mobile phone: +86 13001359170
Email: wljabgf@126.com

Guangquan SU, Postgraduate Student
National Engineering Research Center for Inland Waterway Regulation, School of River and Ocean Engineering,
Chongqing Jiaotong University,
66 Xuefu Road, Nan'an District,
Chongqing 400074, P. R. China
People's Republic of China
Mobile phone: +86 15923274096
E-mail: 984223593@qq.com